

DIFFERENT ACCRETION HEATING OF THE NEUTRON STAR CRUST DURING MULTIPLE OUTBURSTS  
IN MAXI J0556–332

AASTHA S. PARIKH,<sup>1</sup> JEROEN HOMAN,<sup>2,3</sup> RUDY WIJNANDS,<sup>1</sup> LAURA OOTES,<sup>1</sup> DANY PAGE,<sup>4</sup> DIEGO ALTAMIRANO,<sup>5</sup>  
NATHALIE DEGENAAR,<sup>1</sup> EDWARD F. BROWN,<sup>6</sup> EDWARD CACKETT,<sup>7</sup> ANDREW CUMMING,<sup>8</sup> ALEX DEIBEL,<sup>9</sup>  
JOEL K. FRIDRIKSSON,<sup>1</sup> DACHENG LIN,<sup>10</sup> MANUEL LINARES,<sup>11</sup> AND JON M. MILLER<sup>12</sup>

<sup>1</sup>*Anton Pannekoek Institute for Astronomy, University of Amsterdam, Postbus 94249, NL-1090 GE Amsterdam, the Netherlands*

<sup>2</sup>*SRON, Netherlands Institute for Space Research, Sorbonnelaan 2, 3584 CA Utrecht, The Netherlands*

<sup>3</sup>*Eureka Scientific, Inc., 2452 Delmer Street, Oakland, California 94602*

<sup>4</sup>*Instituto de Astronomía, Universidad Nacional Autónoma de México, Mexico D.F. 04510, Mexico*

<sup>5</sup>*Department of Physics and Astronomy, Southampton University, Southampton SO17 1BJ, UK*

<sup>6</sup>*Department of Physics and Astronomy, Michigan State University, 567 Wilson Rd, East Lansing, MI 48864, USA*

<sup>7</sup>*Department of Physics & Astronomy, Wayne State University, 666 W. Hancock St, Detroit, MI 48201, USA*

<sup>8</sup>*Department of Physics and McGill Space Institute, McGill University, 3600 Rue University, Montreal QC, Canada H3A 2T8*

<sup>9</sup>*Astronomy Department, Indiana University, Bloomington, IN 47405*

<sup>10</sup>*Space Science Center, University of New Hampshire, Durham, NH 03824, USA*

<sup>11</sup>*Departament de Física, EEBE, Universitat Politècnica de Catalunya, c/ Eduard Maristany 10, 08019 Barcelona, Spain*

<sup>12</sup>*Department of Astronomy, University of Michigan, 500 Church Street, Ann Arbor, MI 48109, USA*

(Received xx; Revised xx; Accepted xx)

Submitted to ApJ

ABSTRACT

The transient neutron star (NS) low-mass X-ray binary MAXI J0556–332 provides a rare opportunity to study NS crust heating and subsequent cooling for multiple outbursts of the same source. We examine *MAXI*, *Swift*, *Chandra*, and *XMM-Newton* data of MAXI J0556–332 obtained during and after three accretion outbursts of different durations and brightness. We report on new data obtained after outburst III. The source has been tracked up to  $\sim 1800$  d after the end of outburst I. Outburst I heated the crust strongly, but no significant reheating was observed during outburst II. Cooling from  $\sim 333$  eV to  $\sim 146$  eV was observed during the first  $\sim 1200$  d. Outburst III reheated the crust up to  $\sim 167$  eV, after which the crust cooled again to  $\sim 131$  eV in  $\sim 350$  d. We model the thermal evolution of the crust and find that this source required a different strength and depth of shallow heating during each of the three outbursts. The shallow heating released during outburst I was  $\sim 17$  MeV nucleon<sup>-1</sup> and outburst III required  $\sim 0.3$  MeV nucleon<sup>-1</sup>. These cooling observations could not be explained without shallow heating. The shallow heating for outburst II was not well constrained and could vary from  $\sim 0$ – $2.2$  MeV nucleon<sup>-1</sup>, i.e., this outburst could in principle be explained without invoking shallow heating. We discuss the nature of the shallow heating and why it may occur at different strengths and depths during different outbursts.

*Keywords:* accretion, accretion disks – stars: neutron – X-rays : binaries – X-rays: individual (MAXI J0556–332)

## 1. INTRODUCTION

Transient neutron stars (NSs) in low-mass X-ray binaries (LMXBs) are excellent laboratories to study dense matter physics. These systems experience accretion outbursts separated by periods of quiescence. During outbursts, the accreted matter compresses the NS surface, inducing heat-releasing nuclear reactions deep in the crust (Haensel & Zdunik 1990, 2008; Steiner 2012) that disrupt the crust-core thermal equilibrium. Once the source transitions into quiescence the crust cools to restore equilibrium with the core. Tracking this crustal cooling and fitting theoretical models to study its evolution allows us to infer NS crust properties (e.g., Brown & Cumming 2009). So far, eight NS LMXBs that show crustal cooling have been studied (see Wijnands et al. 2017, for a review). In addition to the standard deep crustal heating ( $\rho \sim 10^{12}\text{--}10^{13}$  g cm $^{-3}$ ), a shallow heat source ( $\rho \sim 10^8\text{--}10^{10}$  g cm $^{-3}$ ) is required to explain the observed cooling curve of many of these sources. The origin of this shallow heat source is unknown and is important to resolve because the cooling curve can be used to constrain a number of different aspects of crust physics (such as conductivity of the crust and pasta, and the core specific heat; Brown & Cumming 2009; Horowitz et al. 2015; Cumming et al. 2017). Most systems need  $\sim 1\text{--}2$  MeV nucleon $^{-1}$  of shallow heating to explain their cooling curves (e.g., Degenaar et al. 2014, Parikh et al. 2017; Wijnands et al. 2017).

The transient NS LMXB MAXI J0556–332 (hereafter J0556) was discovered on 2011 January 11 (Matsumura et al. 2011) and exhibited a  $\sim 16$  month outburst. The source showed a second outburst in 2012 that lasted  $\sim 2$  months (Sugizaki et al. 2012) and a third  $\sim 3$  month outburst in 2016 (Negoro et al. 2016). In Figure 1 (top panel) we show the MAXI light curve with all three outbursts. Sugizaki et al. (2013) examined the spectral data obtained using the MAXI, Swift, and RXTE when the source was in outburst, and constrained the source distance to be  $>17$  kpc. Homan et al. (2014, hereafter Ho14) studied the Swift, Chandra, and XMM-Newton spectra of the source after its outbursts and found a distance of  $\sim 45$  kpc. Such a large distance was further supported by the  $46 \pm 15$  kpc distance the same authors obtained when comparing the X-ray colour-colour and hardness-intensity diagram of J0556 with those observed for other, similarly bright ( $\sim$ Eddington limited) NS LMXBs (i.e., the so-called Z sources).

Ho14 studied J0556 in quiescence after outburst I and II and found it to have a very hot NS crust. They showed that outburst II did not seem to reheat the NS crust. Deibel et al. (2015) showed that J0556 released a very large amount of shallow heating during outburst I of  $\sim 10$

MeV nucleon $^{-1}$  to explain its crust cooling evolution, the largest required by any NS LMXB source studied so far. During outburst II, the shallow heating mechanism was inactive or at a much reduced level compared to outburst I. Here we present cooling observations of J0556 after outburst III demonstrating that the source was reheated during this outburst, requiring a small but significant amount of shallow heating. Therefore, the shallow heating mechanism is not just active or inactive but can indeed be active at different strengths.

## 2. OBSERVATIONS, DATA ANALYSIS, AND RESULTS

J0556 has been observed in quiescence by the Swift, Chandra, and XMM-Newton observatories. We use MAXI and the X-ray Telescope (XRT; Burrows et al. 2005) aboard Swift to track the variability of the source during its outbursts. We report on eight new Chandra and XMM-Newton observations of this source. For uniformity, we also reanalyse all observations reported by Ho14. Table 1 shows the log of quiescent observations.

### 2.1. MAXI

The outburst evolution of J0556 was observed using the MAXI/Gas Slit Camera (GSC; Mihara et al. 2011). We downloaded the light curve from the MAXI archive<sup>1</sup> for the 2–4 keV range as Ho14 suggest that this energy range results in the highest signal-to-noise ratio. Similar to their analysis, we remove data that have error bars larger 0.025 counts s $^{-1}$  and apply a 3 day rebinning.

### 2.2. Swift/XRT

Swift/XRT was also used to monitor the evolution of J0556. The raw data were processed with HEASOFT (version 6.17) using xrtpipeline. The light curve and spectra were extracted using XSELECT (version 2.4c). A circular source extraction region with a radius of 40'' was used. For the background extraction region we used an annulus of inner and outer radii 50'' and 80'', respectively.

Four observations after outburst I were combined into one interval to obtain constraints on the earliest crust cooling phase (observation ID [obsID]: 00032452004–00032452007; from 2012 May 7 to 2012 May 11). The Photon Counting mode data from these observations were stacked into a single event file and the spectrum was extracted using the same source and background regions as those used for the light curve. The ancillary response file was generated using xrtrmkarf and the appropriate response matrix file

<sup>1</sup> <http://maxi.riken.jp/top/slist.html>

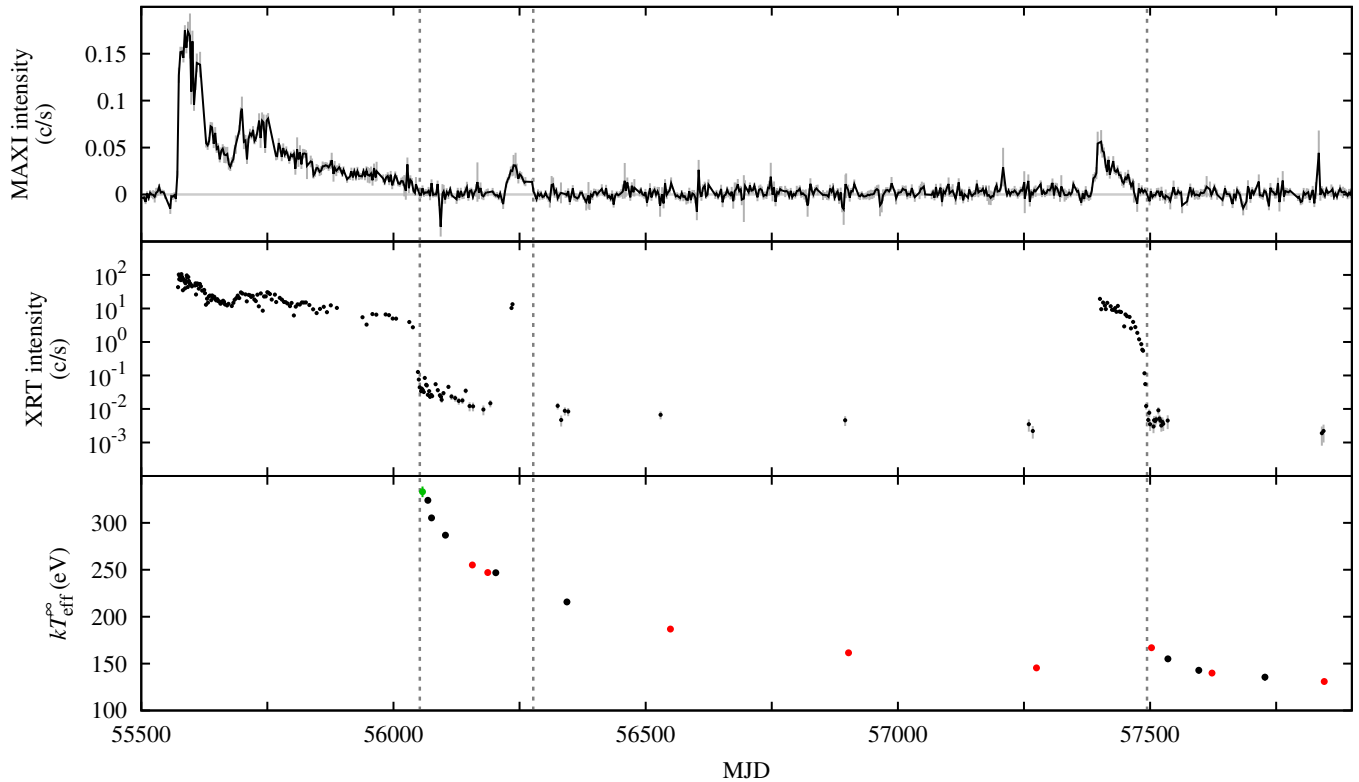


**Figure 1.** Long-term light curves of J0556 from *MAXI*/GSC (top panel, 2–4 keV) and *Swift*/XRT (middle panel, 0.5–10 keV). In the bottom panel we show the temperature evolution of the source during its quiescent periods (the green, black, and red points indicate the *Swift*/XRT, *Chandra*, and *XMM-Newton* data, respectively). The dotted grey lines indicate the time of transition to quiescence after each outburst.

‘swxpc0to12s6\_20110101v014.rmf’ was used. The 0.3–10 keV spectrum was binned to have a minimum of 5 counts per bin using *grppha*.

### 2.3. *Chandra*

J0556 was observed ten times with the *Chandra*/ACIS-S (Garmire et al. 2003) in the FAINT mode using the 1/8 sub-array. Two observations (ObsID: 14429 and 14227; see Table 1 of Ho14) took place during episodes of temporary increases in accretion rate during the first  $\sim 100$  d after the end of outburst I. Since we are only interested in the crust cooling behaviour we do not discuss these data (see Ho14, for more information about these observations). CIAO (version 4.9) was used to process the raw data of the remaining eight observations. We examined the source light curves for possible episodes of background flaring, but none were found. We used circular source extraction regions with a radius of  $2''$ – $3''$  (depending on source brightness). The background extraction region used was an annulus with inner and outer radii  $10''$  and  $20''$ , respectively. The spectra were extracted using *specextract*. The point-source aperture-corrected *arf* files, as generated by

*specextract*, were used. The 0.3–10 keV spectra were grouped using *dmgroup* to have a signal-to-noise ratio of 4.5.

### 2.4. *XMM-Newton*

*XMM-Newton* (Strüder et al. 2001) was used to observe J0556 eight times using all three European Photo Imaging Cameras (EPIC) – MOS1, MOS2, and pn. The raw data were reduced using the Science Analysis System (SAS; version 16.0) and processed using *emproc* and *epproc* for the MOS and pn detectors, respectively. The observations were checked for background flaring by examining the light curves for the  $>10$  keV range for the MOS detectors and 10–12 keV range for the pn detector. Depending on the average source brightness during an observation, we removed data of  $>0.08$ – $0.16$  counts  $s^{-1}$  and data of  $>0.32$ – $0.4$  counts  $s^{-1}$  for the MOS and pn detectors, respectively. Circular source and background extraction regions were used for the spectral extraction. The optimal source region to be used was determined with *eregionanalyse*. Depending on the source brightness, regions of radii  $19''$ – $45''$  were used for the MOS detectors and regions of radii  $19''$ – $37''$  were used for the

pn detector. A background region of radius  $50''$  was used for each observation, placed on the same CCD that the source was located on. The position of the background region as suggested by the `ebkgreg` tool was used. The redistribution matrix file and ancillary response function were generated using `rmfgen` and `arfgen`. The 0.3–10 keV spectra were binned using `specgroup`, with the signal-to-noise ratio set to 4.5.

### 2.5. Spectral Fitting

All *Chandra* and *XMM-Newton* 0.3–10 keV spectra were fit simultaneously in `XSPEC` (version 12.9; Arnaud 1996) using  $\chi^2$  statistics. We used the NS atmosphere model `nsa` (Zavlin et al. 1996). The `nsatmos` model cannot be used as the source was very hot at the start of the cooling phase (see Ho14, for details). The temperature was left free for each individual *XMM-Newton* and *Chandra* observation. However, this parameter was tied between the MOS and pn cameras for a given *XMM-Newton* observation. All the temperatures were converted into the effective temperature measured by an observer at infinity. The mass and radius of the NS were fixed to  $1.4 M_{\odot}$  and 10 km (since in the `nsa` model the surface gravity has only been calculated for this combination and does not give accurate results for other mass and radius values; Zavlin et al. 1996; Heinke et al. 2006). The magnetic field parameter was set to zero (indicating a non-magnetised star). The normalization ( $1/D^2$ ;  $D$  is the distance) and the  $N_{\text{H}}$  were free parameters but were tied between all observations. The  $N_{\text{H}}$  was modeled using `tbnew_feo`<sup>2</sup> with WILM abundances (Wilms et al. 2000) and VERN cross-sections (Verner et al. 1996). The Oxygen and Iron abundances for `tbnew_feo` were fixed to 1.

We use the `pileup` component to model the pile-up in the *Chandra* data<sup>3</sup>. We set the maximum number of photons considered for pile up in a single frame to 3, the grade correction for single photon detection to 1, the PSF fraction is fixed to 0.95, the number of regions and the `FRACEXPO` keyword are both set to 1. We find that the fits are not very sensitive to the alpha parameter (see also Ho14) and we fix this value to 0.6. The frame time, an input parameter for `pileup`, was set to 0.4 s for the *Chandra* observations. To prevent the pile-up model from affecting the *XMM-Newton* data we set the frame time for these observations to a very small value ( $10^{-6}$  s). We also use the multiplicative model `constant` to allow for normalisation offsets between the *Chan-*

*dra* and *XMM-Newton* observatories. For the *Chandra* data we used a constant of 1 and for the various *XMM-Newton* detectors – MOS1, MOS2, and pn the constants were calculated from Table 5 of Plucinsky et al. (2017),  $C_{\text{MOS1}} = 0.983$ ,  $C_{\text{MOS2}} = 1$ ,  $C_{\text{pn}} = 0.904$ .

The simultaneous fit of all the *Chandra* and *XMM-Newton* data resulted in a column density of  $N_{\text{H}} = (3.2 \pm 0.5) \times 10^{20} \text{ cm}^{-2}$  and a distance of  $43.6_{-1.6}^{+0.9}$  kpc. While calculating the error on the temperature we fixed the best fit  $N_{\text{H}}$  and distance values as they are not expected to vary between observations (see also, e.g., Wijmands et al. 2004, Ho14). The parameters from the obtained fit ( $\chi^2_{\nu}/\text{d.o.f.} = 1.02/715$ ) are shown in Table 1. Changing the mass, radius,  $N_{\text{H}}$ , and distance will change the absolute  $kT_{\text{eff}}^{\infty}$  but the trend, which helps us understand crust physics, will not change significantly (e.g., Cackett et al. 2008). The brightest *Chandra* observations had a pile-up fraction of  $\sim 2$  per cent.

Due to the small number of counts per bin in the *Swift*/XRT spectra (0.3–10 keV), they were fit separately with W-statistics (background subtracted Cash statistics) using the same  $N_{\text{H}}$  and distance as used for the *Chandra* and *XMM-Newton* spectral fitting. We allow for a normalisation offset of  $C_{\text{XRT}} = 0.872$  (Plucinsky et al. 2017).

Figure 1 shows the *MAXI* (top panel) and *Swift*/XRT (middle panel) light curves of J0556. The bottom panel of Figure 1 shows the cooling evolution of J0556, suggesting a strong decrease in the  $kT_{\text{eff}}^{\infty}$  after the end of outburst I. Outburst II did not reheat the crust significantly and the cooling appeared to continue along its previous trend (see also Ho14). Overall, the crust cooled from  $\sim 333$  eV to  $\sim 146$  eV, after the outburst I and II. Outburst III caused the crust to be reheated significantly (to  $\sim 167$  eV) and was followed by subsequent cooling (to  $\sim 131$  eV approximately 350 days after the end of this recent outburst).

### 2.6. Modelling the quiescent thermal evolution

We model the outbursts and quiescence of J0556 using the crustal heating/cooling code `NSCOOL` (Page & Reddy 2013; Page 2016). We account for the accretion rate variability during the outbursts and model all three outbursts collectively (using the methods of Ootes et al. 2016, 2017). The transition to quiescence after outburst I occurred on MJD 56052.1 (see Ho14). We use the methodology described by Fridriksson et al. (2010) to calculate the time of transition to quiescence by fitting an exponential to the rapidly decaying trend at the end of the outburst and a straight line to the quiescent points soon after the end of the outburst. We used the *MAXI* and *Swift*/XRT light curve, respectively, for this calcu-

<sup>2</sup> <http://pulsar.sternwarte.uni-erlangen.de/wilms/research/tbabs/>

<sup>3</sup> We use values suggested by the *Chandra* pile-up guide: [http://cxc.harvard.edu/ciao/download/doc/pileup\\_abc.pdf](http://cxc.harvard.edu/ciao/download/doc/pileup_abc.pdf)

**Table 1.** Log of the quiescent observations.<sup>a</sup>

Instrument	ObsID	Days since end of outburst I	Exposure time <sup>b</sup> (ksec)	$kT_{\text{eff}}^{\infty}$ (eV)	$F_{\text{X}}$ ( $\times 10^{-14}$ erg cm <sup>-2</sup> s <sup>-1</sup> )	$L_{\text{X}}$ ( $\times 10^{33}$ erg s <sup>-1</sup> )	
<i>After Outburst I</i>							
1	<i>Swift</i>	Interval 1 <sup>c</sup>	5.4	10.1	$333.1 \pm 5.5$	$109.7 \pm 6.6$	$249.5 \pm 15.1$
2	<i>Chandra</i>	14225	16.0	9.2	$324.1 \pm 2.5$	$106.3 \pm 3.6$	$241.9 \pm 8.3$
3	<i>Chandra</i>	14226	23.3	9.1	$305.4 \pm 2.5$	$79.7 \pm 2.8$	$181.2 \pm 6.3$
4	<i>Chandra</i>	14433	51.0	18.2	$286.9 \pm 1.9$	$62.4 \pm 1.8$	$142.0 \pm 4.0$
5	<i>XMM-Newton</i>	0700380901	104.3	28.2, 27.6, 21.5	$255.2 \pm 0.9$	$37.9 \pm 0.6$	$86.2 \pm 1.3$
6	<i>XMM-Newton</i>	0700381201	134.9	24.4, 23.7, 17.5	$247.1 \pm 1.0$	$32.6 \pm 0.7$	$74.1 \pm 1.4$
7	<i>Chandra</i>	14434	150.8	18.2	$246.8 \pm 2.1$	$33.5 \pm 1.3$	$76.2 \pm 2.8$
<i>After Outburst II</i>							
8	<i>Chandra</i>	14228	291.7	22.7	$215.8 \pm 2.2$	$19.1 \pm 0.8$	$43.5 \pm 1.9$
9	<i>XMM-Newton</i>	0725220201	496.8	44.3, 42.3, 34.9	$186.8 \pm 1.0$	$10.2 \pm 0.2$	$23.2 \pm 0.6$
10	<i>XMM-Newton</i>	0744870201	850.1	77.3, 78.6, 59.9	$161.5 \pm 0.8$	$5.5 \pm 0.1$	$12.6 \pm 0.3$
11	<i>XMM-Newton</i>	0762750201	1222.6	83.9, 72.3, 57.5	$145.4 \pm 1.0$	$3.5 \pm 0.1$	$7.9 \pm 0.3$
<i>After Outburst III</i>							
12	<i>XMM-Newton</i>	0784390301	1450.7	20.4, 18.6, 18.6	$166.9 \pm 1.8$	$6.9 \pm 0.5$	$15.7 \pm 1.1$
13	<i>Chandra</i>	18335	1483.2	27.3	$155.1 \pm 2.8$	$4.8 \pm 0.4$	$10.9 \pm 1.0$
14	<i>Chandra</i>	18336	1544.3	27.1	$142.9 \pm 3.3$	$3.4 \pm 0.5$	$7.8 \pm 1.0$
15	<i>XMM-Newton</i>	0784390401	1570.6	45.9, 41.3, 39.5	$139.9 \pm 1.4$	$3.0 \pm 0.1$	$6.7 \pm 0.3$
16	<i>Chandra</i>	18337	1675.5	27.3	$135.6 \pm 3.5$	$2.6 \pm 0.3$	$6.0 \pm 0.7$
17	<i>XMM-Newton</i>	0782670201	1793.1	61.0, 58.3, 36.7	$130.9 \pm 1.5$	$2.3 \pm 0.1$	$5.1 \pm 0.3$

<sup>a</sup> All errors are  $1\sigma$ . The distance and  $N_{\text{H}}$  were fixed to 43.6 kpc and  $3.2 \times 10^{20}$  cm<sup>-2</sup>. The unabsorbed fluxes and luminosities are quoted for 0.5–10 keV.

<sup>b</sup> The *XMM-Newton* effective exposure times have been displayed as ‘MOS1, MOS2, pn’.

<sup>c</sup> See Section 2.2.

lation after outburst I and II and determined the transition time to be MJD 56277.4 and MJD 57494.2.

We account for accretion rate variability during the outbursts by tracking the daily average rate, which is determined from the daily averaged *MAXI* and *Swift*/XRT count rates. If data from both instruments are available on the same day, the *Swift*/XRT data are used. Sugizaki et al. (2013) report the bolometric flux ( $F_{\text{bol}}$ ) from J0556 at six different instances during the first outburst (no such reports are available for the other two outbursts). We use these values to calculate a count rate to  $F_{\text{bol}}$  conversion constant for the *MAXI* and *Swift*/XRT data using count rates from the same days as the six reported  $F_{\text{bol}}$  values. This constant was calculated for each of the six observations for both instruments and the final constant used for each instrument was the averaged value. The obtained constants are  $C_{\text{MAXI}} = 2.353 \times 10^{-8}$  erg

cm<sup>-2</sup> count<sup>-1</sup> and  $C_{\text{Swift}} = 4.957 \times 10^{-11}$  erg cm<sup>-2</sup> count<sup>-1</sup>. The individual count rate to  $F_{\text{bol}}$  conversion constants differ at most by a factor of  $\sim 2$  from each other. We tested our NSCOOL model results by using these minimum or maximum calculated individual conversion constant values (instead of the averaged ones) for all three outbursts as well as by using different values for different outbursts. We find that this only inconsequentially changes our inferred NS parameters without affecting our main conclusions. The  $F_{\text{bol}}$  was used to calculate the daily average accretion rate using

$$\dot{M} = \frac{F_{\text{bol}} 4\pi D^2}{\eta c^2}$$

where  $\eta$  ( $= 0.2$ ) indicated the efficiency factor and  $c$  is the speed of light. Using this we obtained the fluences of

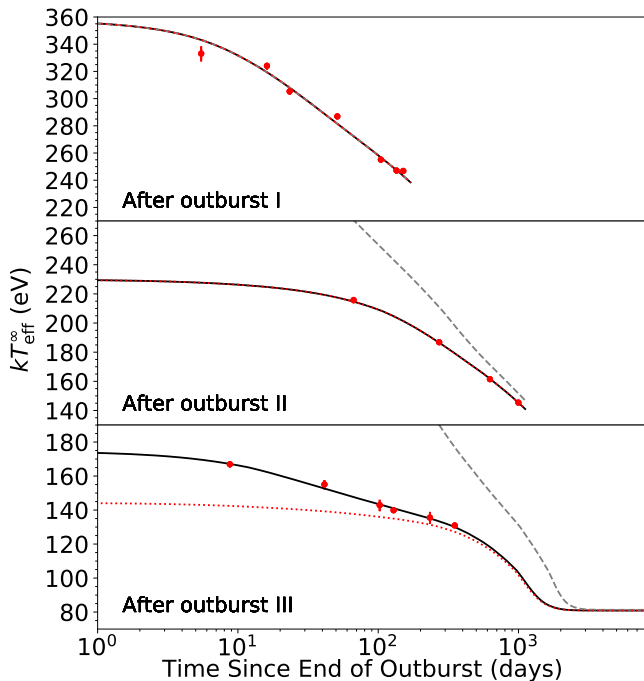


**Figure 2.** The  $kT_{\text{eff}}^{\infty}$  evolution of J0556 in quiescence with the cooling curves calculated using NSCOOL. The solid black line shows the best fit model with all three outbursts having different shallow heating parameters. The dashed grey line shows the outcome if the same shallow heating parameters as inferred for outburst I were used for all three outbursts. The dotted red line shows the model when no shallow heating was assumed to be active during outburst II and III.

the three outbursts to be  $\sim 4.3 \times 10^{-2}$  erg cm $^{-2}$ ,  $\sim 2.1 \times 10^{-3}$  erg cm $^{-2}$ ,  $\sim 4.4 \times 10^{-3}$  erg cm $^{-2}$ , respectively.

The NS mass and radius used for the NSCOOL models are the same as those used for the spectral fits. The distance used is that calculated from the best fit to the spectra (Section 2.5). The NSCOOL adjustable parameters are the impurity factor in the crust ( $Q_{\text{imp}}$ ), the column depth of light elements in the envelope ( $y_{\text{light}}$ ), the core temperature prior to the first outburst ( $T_0$ ), and the strength ( $Q_{\text{sh}}$ ) and depth ( $\rho_{\text{sh}}$ ) of the shallow heating. We model the shallow heating with different parameters during each outburst. Furthermore, we also allow the envelope composition of the crust to vary for each outburst (Ootes et al. 2017). The best fit is found using a  $\chi^2$  minimisation algorithm and all errors are calculated for the  $1\sigma$  confidence range.

Our modelling shows that heating only by deep crustal reactions (in combination with changes in the envelope composition) cannot explain the observations of J0556. A significant amount of shallow heating is necessary to

**Table 2.** Shallow heating parameters from NSCOOL.

Outburst	$Q_{\text{sh}}$ (MeV nucleon $^{-1}$ )	$\rho_{\text{sh}}$ ( $\times 10^9$ g cm $^{-3}$ )
I	$17.0^{+2.2}_{-0.7}$	$5.3^{+0.2}_{-0.5}$
II <sup>a</sup>	0	–
	$2.2 \pm 0.7$	$33.5 \pm 0.8$
III	$0.33 \pm 0.03$	$1.6 \pm 1.3$

<sup>a</sup> Note that the parameters for outburst II are given for a range of values.

explain the data.  $Q_{\text{sh}} \sim 17$  MeV nucleon $^{-1}$  is needed to explain the high temperatures after outburst I. The best fit model ( $\chi^2_{\nu}/\text{d.o.f.} = 2.8/9$ ) is shown by the solid black line in Figure 2 and the parameters are listed in Table 2. Outburst II and III cannot be explained with the same shallow heating as required for outburst I, not even if the envelope composition is allowed to change (Brown et al. 2002). The dotted gray line in Figure 2 shows a model that assumes that during all three outbursts the shallow heating mechanism released  $Q_{\text{sh}} \sim 17$  MeV nucleon $^{-1}$ , clearly showing that this would result in much hotter crusts than what we have observed. Outburst III could be modelled with  $Q_{\text{sh}} \sim 0.3$  MeV nucleon $^{-1}$  at shallower depths than that required for outburst I. Outburst III could not be modelled without shallow heating. This is shown by the dotted red line in Figure 2 which indicates a model for which we assumed that the shallow heating mechanism was not active during outburst II and III. This model shows that outburst II can be explained without shallow heating. However, the uncertainties on the shallow heating parameters after outburst II are large, ranging from (a) no shallow heating ( $Q_{\text{sh}} \sim 0$  MeV nucleon $^{-1}$ ) when this heating source is at relatively shallow depths (i.e. the  $\rho_{\text{sh}}$  corresponding to outburst I or outburst III) as well as (b) a large  $Q_{\text{sh}} \sim 2.2$  MeV nucleon $^{-1}$  very deep in the crust (at  $\rho_{\text{sh}} \sim 33.5 \times 10^9$  g cm $^{-3}$ ). This is because the  $Q_{\text{sh}}$  and  $\rho_{\text{sh}}$  are correlated and the modelled curve from these two possibilities have a very similar shape.

In addition to constraining the shallow heating parameters, we found a core temperature of  $T_0 = (5.5 \pm 0.4) \times 10^7$  K. Assuming a  $Q_{\text{imp}} = 1$  throughout the crust fit the data well. Increasing the  $Q_{\text{imp}}$ , to  $\sim 20$  as suggested by Horowitz et al. (2015), in the pasta layer (which extends from  $\rho \sim 10^{13}$  g cm $^{-3}$  to the crust-core boundary) reduced the fit quality, indicating that the crust of this source has a high thermal conductivity throughout.

Our best fit model indicates that a relatively light envelope is necessary after outburst I ( $y_{\text{light}} \sim 3.1 \times 10^9$  g

$\text{cm}^{-2}$ ). The data after outburst I cannot be adequately fit using a heavy element envelope as the light elements are necessary to raise the effective temperature to that we observe. The envelope composition systematically raises or drops the observed trend whereas a change in the shallow heating changes the slope of the trend itself, therefore they are only partially degenerate in determining the cooling trend. The best fit indicates that a similar envelope composition ( $[2.1 - 3.1] \times 10^9 \text{ g cm}^{-2}$ ) is present after all three outbursts. Further extensive investigation into the NSCOOL parameters is not the aim of our paper.

### 3. DISCUSSION

We studied the NS LMXB J0556 in quiescence. Since the NS mass, radius, and distance remain the same between outbursts, studying the source after multiple outbursts allows us to investigate which parameters affecting the heating and cooling behaviour of the crust may change. As reported by Ho14, we found a strongly heated crust after outburst I. The amount of shallow heating during outburst I was very large, at  $Q_{\text{sh}} \sim 17 \text{ MeV nucleon}^{-1}$ . During outburst II the shallow heating mechanism may have been inactive (see also Deibel et al. 2015, for similar results of outburst I and II). However, it should be noted that the first pointing was obtained long after the end of outburst II ( $\sim 70 \text{ d}$ ) and  $Q_{\text{sh}}$  could not be constrained well. Up to  $\sim 2.2 \text{ MeV nucleon}^{-1}$  was still allowed during this outburst if the heating occurred at much larger depths. We present new quiescent observations after the end of outburst III. Shallow heating (at  $\sim 0.3 \text{ MeV nucleon}^{-1}$ ) needs to have been active during outburst III to explain the reheating we observed after the end of the outburst since the deep crustal reactions alone cannot account for this reheating. Based on the well constrained shallow heating parameters found after outburst I and III we find that this heating mechanism may release different amounts of heat per accreted nucleon during different outbursts and may not be simply active or inactive (as could still be the case after the study by Deibel et al. 2015).

The origin of shallow heating remains unknown and thus also why its strength varies during different outbursts. One possibility (as suggested by Inogamov & Sunyaev 2010) is that the shallow heating originates from the dissipation of the accretion-generated  $g$ -modes in the ocean (i.e., the melted crust). Based on the  $kT_{\text{eff}}^{\infty}$ , we find that the ocean is deeper during outburst II than outburst III. If the shallow heat source is placed at this

ocean-solid crust interface then our models indicate that more shallow heat is required during outburst III than outburst II, suggesting that the strength of heat deposition is unlikely to vary with the depth of the ocean (as suggested by Deibel 2016).

It is interesting to note that the strength of the shallow heating seems to correlate with the outburst fluences ( $Q_{\text{sh}}$  decreases from  $\sim 17 \text{ MeV nucleon}^{-1}$  to  $\sim 0.3 \text{ MeV nucleon}^{-1}$  when the fluence decreases from  $\sim 4.3 \times 10^{-2} \text{ erg cm}^{-2}$  to  $\sim 4.4 \times 10^{-3} \text{ erg cm}^{-2}$ ). However, even if true for J0556, this cannot be extrapolated to other sources. Another NS LMXB XTE J1701–462 experienced an outburst in 2006/2007 with a similar fluence to outburst I of J0556 (Fridriksson et al. 2010, 2011; see Ho14 for details), but J0556 needs  $Q_{\text{sh}} \sim 17 \text{ MeV nucleon}^{-1}$  to explain its cooling data whereas XTE J1701–462 needs only  $Q_{\text{sh}} \sim 0.1 \text{ MeV nucleon}^{-1}$  (Page & Reddy 2013). Therefore, across sources there is another, unknown parameter that sets the strength of the shallow heating.

Using our NSCOOL models we attempted to discern if the observed crust cooling currently follows the cooling trend defined by outburst I or if the reheating from outburst III still influences the crust temperature. We find that a model which only includes heating from outburst I, slightly undershoots our most recently obtained data point suggesting that the crust might not have yet returned to the original cooling trend. However, due to uncertainties in the data and the modelling we cannot conclusively say if this is indeed the case. Future *Chandra* observations will clarify this as well as probe the pasta layer present deeper in the crust.

### ACKNOWLEDGEMENTS

AP, RW, and LO are supported by a NWO Top Grant, Module 1, awarded to RW. JH acknowledges financial support from NASA grants GO6-17033X, NNX16AH25G, and NNX15AJ36G. ND is supported by an NWO Vidi grant. DP is supported by the Consejo Nacional de Ciencia y Tecnología with a CB-2014-1 grant #240512. DA acknowledges support from the Royal Society. This work was benefitted from support by the National Science Foundation under Grant No. PHY-1430152 (JINA Center for the Evolution of the Elements). ML is supported by EU’s Horizon 2020 programme (Marie Skłodowska-Curie Fellowship; grant nr. 702638). The authors wish to thank Mike Nowak for discussions on applying the Chandra pile-up model.

### REFERENCES

- Arnaud, K. 1996, in *Astronomical Data Analysis Software and Systems V*, Vol. 101, 17
- Brown, E. F., Bildsten, L., & Chang, P. 2002, *ApJ*, 574, 920

- Brown, E. F., & Cumming, A. 2009, *ApJ*, 698, 1020
- Burrows, D. N., Hill, J., Nousek, J., et al. 2005, *Space Science Reviews*, 120, 165
- Cackett, E. M., Wijnands, R., Miller, J. M., Brown, E. F., & Degenaar, N. 2008, *ApJ Letters*, 687, L87
- Cumming, A., Brown, E. F., Fattoyev, F. J., et al. 2017, *PhRvC*, 95, 025806
- Degenaar, N., Medin, Z., Cumming, A., et al. 2014, *ApJ*, 791, 47
- Deibel, A. 2016, *ApJ*, 832, 44
- Deibel, A., Cumming, A., Brown, E. F., & Page, D. 2015, *ApJ Letters*, 809, L31
- Fridriksson, J. K., Homan, J., Wijnands, R., et al. 2010, *ApJ*, 714, 270
- . 2011, *ApJ*, 736, 162
- Garmire, G. P., Bautz, M. W., Ford, P. G., Nousek, J. A., & Ricker, G. 2003, in *Proceedings of SPIE*, Vol. 4851, 28–44
- Haensel, P., & Zdunik, J. 1990, *A&A*, 227, 431
- . 2008, *A&A*, 480, 459
- Heinke, C. O., Rybicki, G. B., Narayan, R., & Grindlay, J. E. 2006, *ApJ*, 644, 1090
- Homan, J., Fridriksson, J. K., Wijnands, R., et al. 2014, *ApJ*, 795, 131
- Horowitz, C., Berry, D., Briggs, C., et al. 2015, *Phys. Rev. Lett.*, 114, 031102
- Inogamov, N., & Sunyaev, R. 2010, *Astronomy Letters*, 36, 848
- Matsumura, T., Negoro, H., Suwa, F., et al. 2011, *ATel*, 3102, 1
- Mihara, T., Nakajima, M., Sugizaki, M., et al. 2011, *PASJ*, 63, S623
- Negoro, H., Nakajima, M., Ueno, T. F. S., et al. 2016, *ATel*, 8513
- Ootes, L. S., Page, D., Wijnands, R., & Degenaar, N. 2016, *MNRAS*, 461, 4400
- . 2017, submitted
- Page, D. 2016, NSCool: Neutron star cooling code, *Astrophysics Source Code Library*, ascl:1609.009
- Page, D., & Reddy, S. 2013, *Phys. Rev. Lett.*, 111, 241102
- Parikh, A. S., Wijnands, R., Degenaar, N., et al. 2017, *MNRAS*, 466, 4074
- Plucinsky, P. P., Beardmore, A. P., Foster, A., et al. 2017, *A&A*, 597, A35
- Steiner, A. W. 2012, *Phys. Rev. C*, 85, 055804
- Strüder, L., Briel, U., Dennerl, K., et al. 2001, *A&A*, 365, L18
- Sugizaki, M., Matsuoka, M., Negoro, H., et al. 2012, *ATel*, 4524, 1
- Sugizaki, M., Yamaoka, K., Matsuoka, M., et al. 2013, *PASJ*, 65, 58
- Tsujimoto, M., Guainazzi, M., Plucinsky, P. P., et al. 2011, *A&A*, 525, A25
- Verner, D., Ferland, G., Korista, K., & Yakovlev, D. 1996, *ApJ*, 465
- Wijnands, R., Degenaar, N., & Page, D. 2017, to appear in a JOAA special issue
- Wijnands, R., Homan, J., Miller, J. M., & Lewin, W. H. 2004, *ApJ Letters*, 606, L61
- Wilms, J., Allen, A., & McCray, R. 2000, *ApJ*, 542, 914
- Zavlin, V., Pavlov, G., & Shibanov, Y. A. 1996, *A&A*, 315, 141